# Evolution of pore-fracture system across maturity and implication for carbon dioxide sequestration in lacustrine shale

Xin Tian[1], Zhejun Pan[1], Yeping Ji[2], Mehdi Ostadhassan[1], Bo Liu[1], Mengdi Sun[1, 4, *]

[1]*National Key Laboratory of Continental Shale Oil, Northeast Petroleum University, Daqing 163318, P. R. China*

[2]*Commonwealth Scientific and Industrial Research Organisation, Perth, WA 6151, Australia*

[3]*Institute of Geosciences, Marine and Land Geomechanics and Geotectonics, Christian-Albrechts-Universität, Kiel 24118, Germany*

[4]*Heilongjiang Provincial Key Laboratory of Continental Shale Oil, Daqing 163712, P. R. China*

E-mail address: 228001010018@stu.nepu.edu.cn (X. Tian); zhejun.pan@nepu.edu.cn (Z. Pan); tim.yeping@gmail.com (Y. Ji); mehdi.ostadhassan@gmail.com (M. Ostadhassan); liubo@nepu.edu.cn (B. Liu); sunmd@nepu.edu.cn (M. Sun).

[*]Corresponding author (ORCID: 0000-0002-3557-3939 (M. Sun))

***Tian, X., Pan, Z., Ji, Y., Ostadhassan, M., Liu, B., Sun, M. Evolution of pore-fracture system across maturity and implication for carbon dioxide sequestration in lacustrine shale. Advances in Geo-Energy Research, 2026, 19(1): 83-96.***

**The link to this file is:** https://doi.org/10.46690/ager.2026.01.07

## Appendix A: Supplementary figure and table

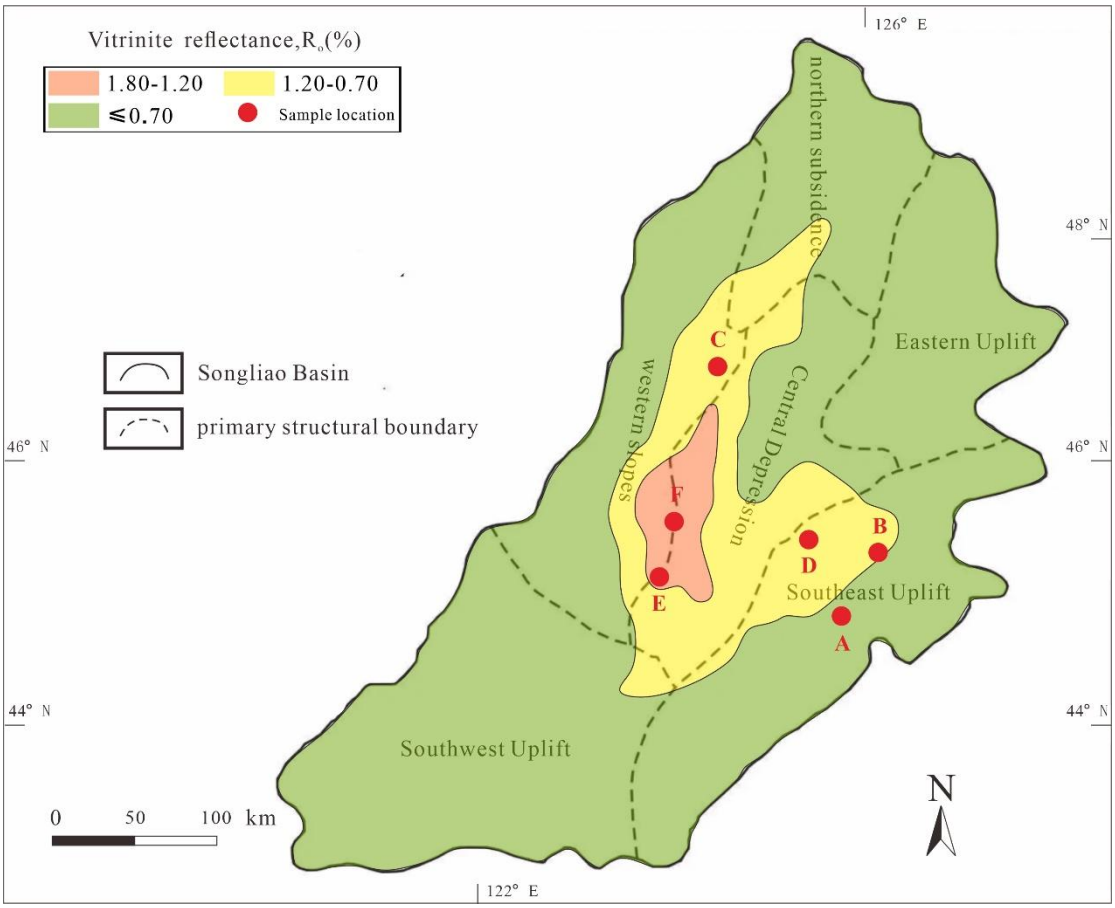


**Fig. S1.** The location of the wells where the samples were collected from the Qingshankou Formation in the Songliao Basin, northeast China.

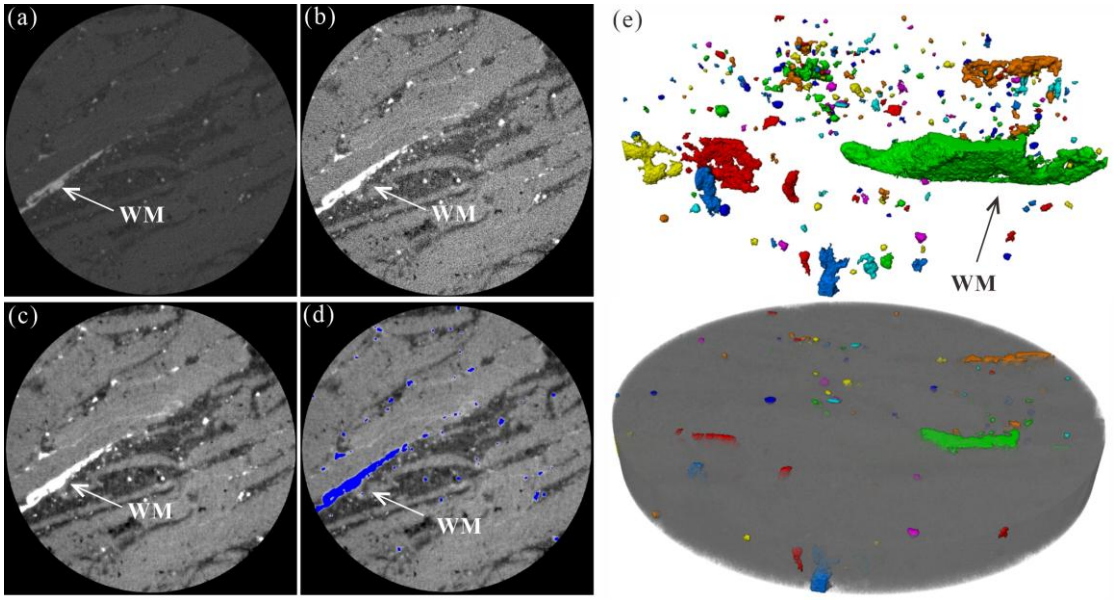


**Fig. S2.** CT image processing: (a) original image, (b) gray value optimization, (c) noise reduction, (d) threshold segmentation, and (e) skeleton structure and pores filled with WM of shale sample.

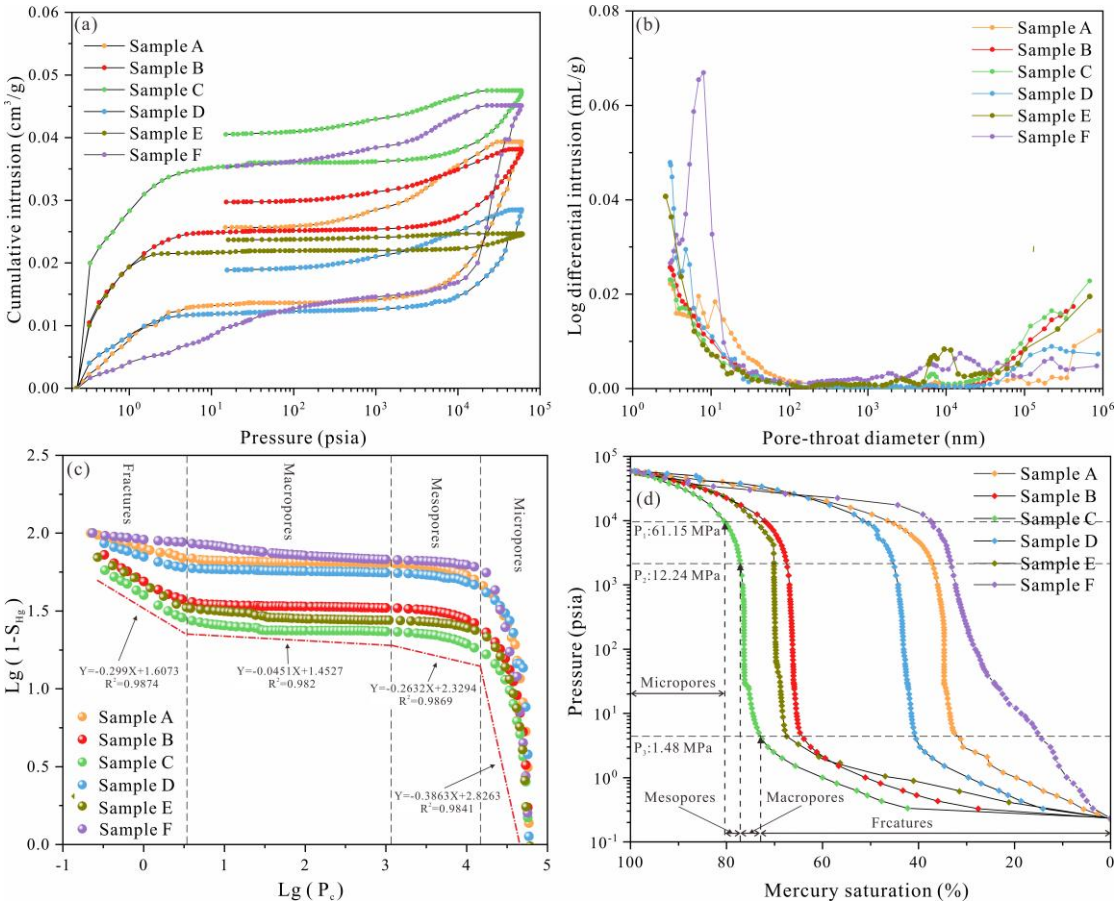


**Fig. S3.** (a) Mercury intrusion-extrusion curves for six samples, (b) Log differential intrusion vs. pore-throat diameter from MICP for six samples, (c) Fractal characteristics of six shale samples, and (d) Inflection point of mercury injection curves for six shale samples. The dotted lines in (c) and (d) indicate the inflection point of intrusion mercury saturation curve and fractal characteristic curves.

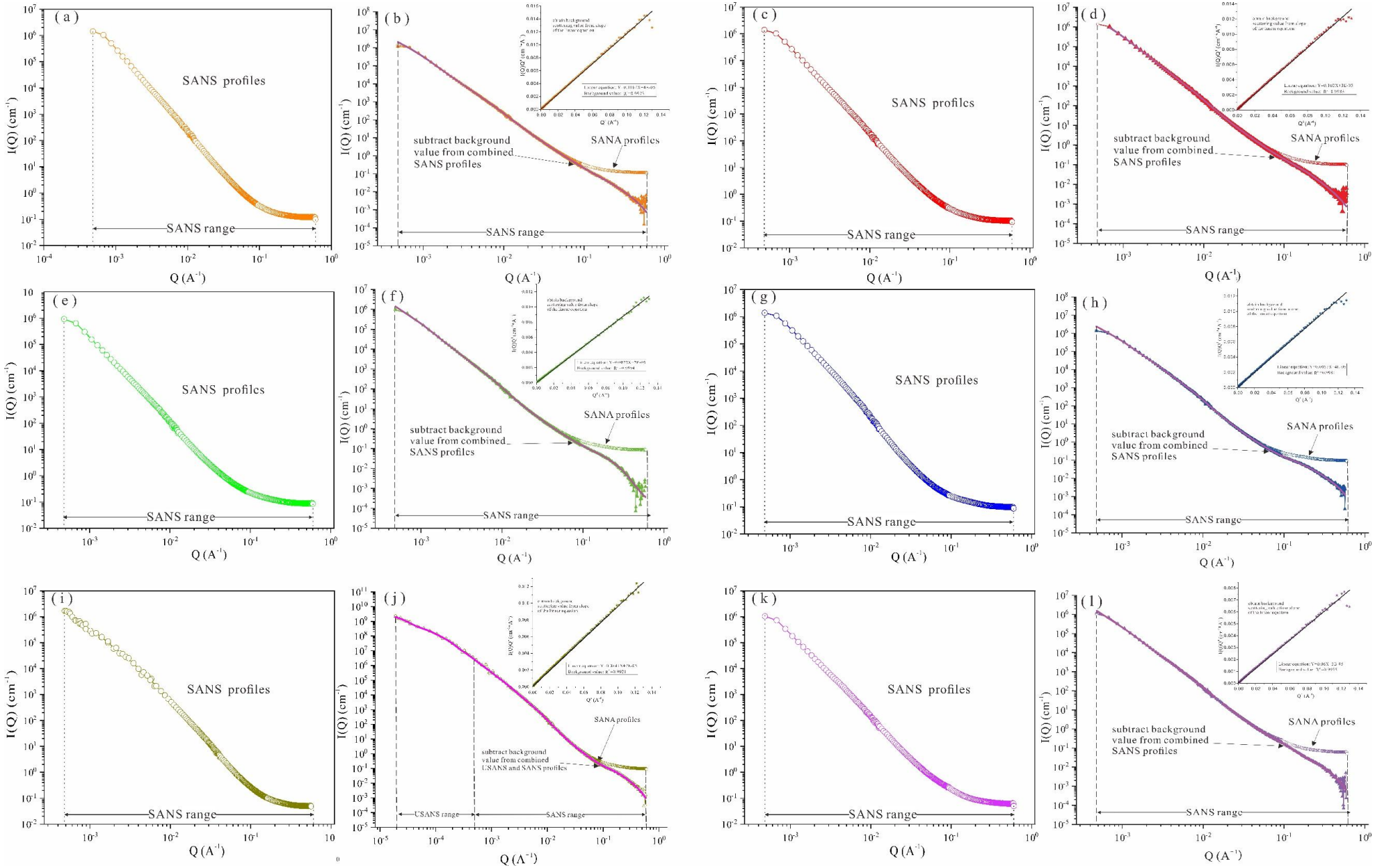


**Fig. S4.** The left panels (a, c, e, g, i, and k) of display the combined SANS and USANS raw scattering profiles for each shale sample. The right panels (b, d, f, h, j, and l) of display the plot of $Q^4I(Q)$ vs. $Q^4$ and (U)SANS profiles of each sample corrected for background. (a-b) sample A, (c-d) sample B, (e-f) sample C, (g-h) sample D, (i-j) sample E, and (k-l) sample F.

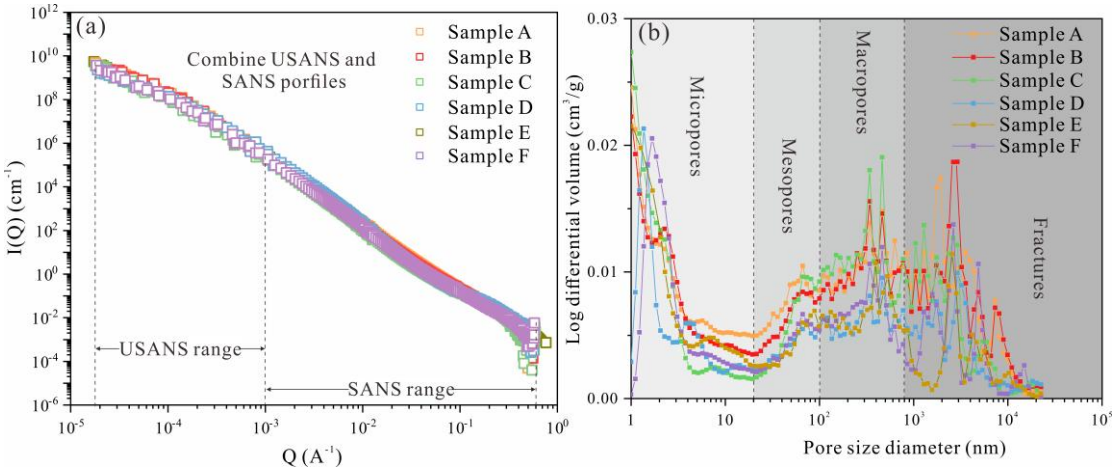


**Fig. S5.** (a) (U)SANS profiles of six samples corrected for background and (b) comparison of pore size volume distribution obtained from (U)SANS.

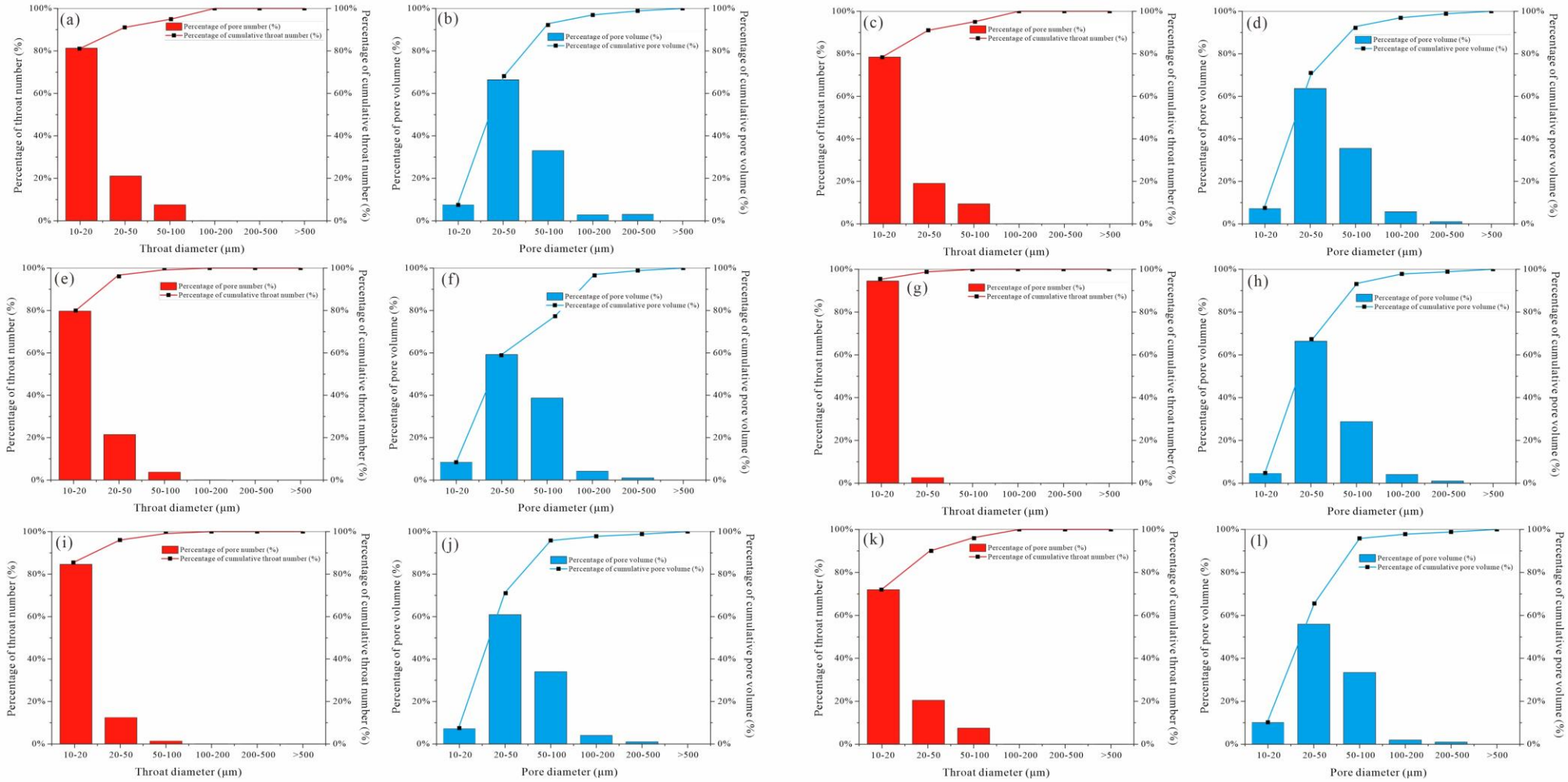


**Fig. S6.** Histogram of throat diameter (a, c, e, g, i, k), pore diameter (b, d, f, h, j, l) of shale pore network model. (a-b) sample A, (c-d) sample B, (e-f) sample C, (g-h) sample D, (i-j) sample E, and (k-l) sample F.

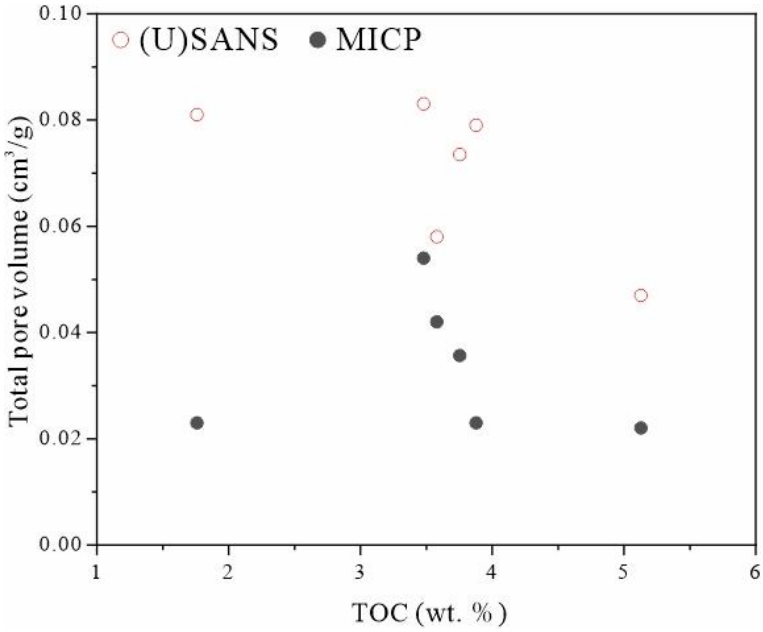


**Fig. S7.** Relationship between TOC and total pore volume of six shale samples with different thermal maturity.

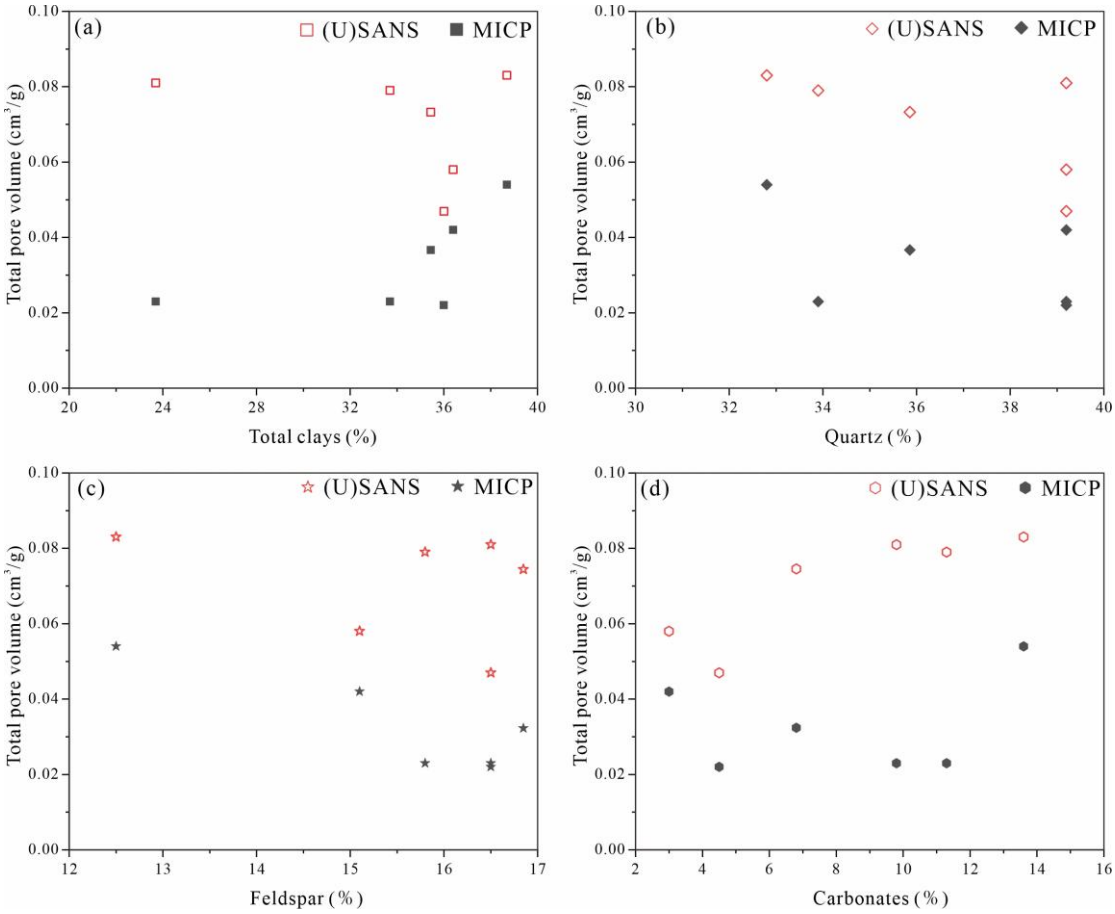


**Fig. S8.** Plots showing the relationship of mineral compositions with total pore volume for the studied Qingshankou shales. (a) Total clays, (b) Quartz, (c) Feldspar, and (d) Carbonates.

Table S1. General mineralogical, geochemical and neutron scattering length density (SLD) properties of the Qingshankou samples used in this study.

| Sample | Depth (m) | Quantitative analysis of whole-rock minerals (wt.%) | | | | | | | TOC (wt.%) | $R_o$ (%) | SLD ($\times 10^{10}$ cm$^{-2}$) |
|---|---|---|---|---|---|---|---|---|---|---|---|
| | | Clays | Quartz | K-feldspar | Plagioclase | Calcite | Dolomite | Pyrite | | | |
| A | 1,067.19 | 38.7 | 32.8 | 0.9 | 11.6 | 0.0 | 13.6 | 2.4 | 3.48 | 0.58 | 4.03 |
| B | 1,625.93 | 33.7 | 33.9 | 0.7 | 15.1 | 0.1 | 11.2 | 5.3 | 3.88 | 0.73 | 4.01 |
| C | 2,315.42 | 23.7 | 39.2 | 0.0 | 16.5 | 9.8 | 7.8 | 3.0 | 1.76 | 0.86 | 4.02 |
| D | 2,038.37 | 36.0 | 39.2 | 0.0 | 16.5 | 2.1 | 2.4 | 3.8 | 5.13 | 0.98 | 4.07 |
| E | 2,459.50 | 36.7 | 34.9 | 0.0 | 16.9 | 0.0 | 6.5 | 5.0 | 3.78 | 1.32 | 4.09 |
| F | 2,347.28 | 36.4 | 39.2 | 0.0 | 15.1 | 3.0 | 0.0 | 6.3 | 3.58 | 1.52 | 4.11 |

Table S2. Pore structure parameters of micropore, mesopore, macropore and fracture by (U)SANS techniques.

| Sample | Micropores | | Mesopores | | Macropores | | Fractures | |
|---|---|---|---|---|---|---|---|---|
| | Porosity (%) | SSA ($m^2/g$) | Porosity (%) | SSA ($m^2/g$) | Porosity (%) | SSA ($m^2/g$) | Porosity (%) | SSA ($m^{2/}g$) |
| A | 2.37 | 12.14 | 1.10 | 4.76 | 1.83 | 3.26 | 2.11 | 2.57 |
| B | 2.41 | 10.62 | 0.84 | 5.22 | 2.04 | 3.21 | 1.94 | 2.03 |
| C | 2.76 | 10.26 | 0.75 | 3.61 | 2.29 | 1.84 | 1.82 | 1.68 |
| D | 1.34 | 15.13 | 0.49 | 4.24 | 1.33 | 3.11 | 0.99 | 1.55 |
| E | 1.58 | 13.97 | 0.49 | 3.21 | 1.35 | 3.85 | 1.19 | 0.95 |
| F | 2.04 | 18.31 | 0.67 | 4.87 | 1.45 | 3.31 | 1.35 | 0.44 |

*SSA = Specific surface area.